Interlayer Structure and Bonding in Nonswelling Primary Amine Intercalated Clays

H. Chris. Greenwell,[†] Matthew J. Harvey,[†] Pascal Boulet,[†,§] Allen A. Bowden,[‡] Peter V. Coveney,*[,†] and Andy Whiting[‡]

Centre for Computational Science, Department of Chemistry, University College of London, 20 Gordon Street, London WC1H OAJ, United Kingdom, and Department of Chemistry, University of Durham, South Road, Durham DH1 3LE, United Kingdom

Received February 22, 2005; Revised Manuscript Received April 29, 2005

ABSTRACT: Preparation of industrially useful clay−polymer nanocomposite materials often requires the dispersal of clay particles within a polymer matrix. The degree to which the clay particles may be dispersed has an effect on the resultant properties of the material, and the clay is often rendered organophilic using alkylammonium species to facilitate incorporation of polymer. The use of a low molecular weight poly(propylene) oxide diamine is investigated as a reagent for controlling the separation between layers in smectite clays and therefore the extent to which the clay tactoid may be dispersed. The arrangement and interactions of the amine species in the interlayer region are investigated through analysis by both experimental methods and computer simulation, which gives insight into coordination mechanisms within the organoclay. Infrared spectroscopy indicates the presence of extensive hydrogen bonding within the amine−clay interlayer. Some of the amine species were found to intercalate in a nonprotonated state, resulting in strong hydrogen-bonding interactions between amine and ammonium groups. Large-scale classical molecular dynamics simulation shows that the amine groups do not interact strongly with the clay sheets, in contradistinction to ammonium groups. The effect of simulation cell size was considered, and in the limit of zero finite size effects, physically realistic undulations are observed within the individual clay sheets.

1. Introduction

The enhanced thermochemical and mechanical properties of a polymer containing dispersed clay platelets has resulted in these clay−polymer composite materials receiving much attention, from both academia and industry.[1] Clay minerals are layered aluminosilicates consisting of stacks of negatively charged two-dimensional sheets, the combined width of the interlayer space and sheet lying in the nanometer range, so that polymer intercalated between these sheets is entrained within a nanosized domain (at least in one dimension). This has resulted in these materials being described as nanocomposites, with the nanoscale interactions appearing to confer "special" properties relative to traditional composites. In particular, substantially less clay filler is required to give the same mechanical, electrical and/or thermal properties as conventional fillers.[2] However, recent work indicates that the effective volume occupied by the clay filler may, in fact, approach that of conventional fillers due to the strong interactions between the clay platelets and a "coating" of tightly bound polymer.[3] The actual volume of the effective clay-based filler is thus substantially greater than that of the clay platelet alone.[3] Much of the current literature is concerned with the preparation of clay−polymer systems where the volume of clay present in the polymer is in the region of 5%. However, we have a long-standing interest in materials where the clay fraction is substantially higher, an area of research of particular interest to the oil field industry.[4−7]

The preparation of clay−polymer nanocomposites is hindered due to the presence of small, highly charged inorganic cations, such as Na^+ and Ca^{2+}, within the interlayer of untreated clays. There are at least two problems associated with these inorganic cations. First, the inorganic cations and their associated hydration spheres create an organophobic environment unfavorable to the adsorption and intercalation of most organic molecules, within the interlayer region. Second, if the water of hydration is removed, the interlayer spacing "collapses" and the high, unscreened electrostatic charge of the cations holds, or "pins", the negatively charged clay sheets together, preventing ingress of polymer material and concomitant exfoliation of the clay sheets.

A technique often used to circumvent this problem is to render the clay interlayer region organophilic, thereby allowing adsorption of organic polymers and subsequent exfoliation, via exchange of the hydrated cations with hydrophobic organoammonium cations.[8] Normally this exchange reaction is carried out using quaternary organoammonium salts with long pendant hydrocarbon groups, which maximize the organophilic nature of the interlayer.[9] Recently, there has been increased interest in the use of primary amines for the preparation of clay−polymer nanocomposites with modified adsorption properties and morphologies.[10−12] These are reviewed in more detail in section 2.

Clay minerals, especially when intercalated by organic molecules, are disordered and as a result extremely difficult to characterize accurately. In many papers the only form of analyses presented are powder X-ray diffraction (PXRD) and thermogravimetric analysis (TGA), which give the interlayer spacing and organic/water content of the composite, respectively. Fourier

[†] University College of London.
[‡] University of Durham.
[§] Present address: MADIREL, UMR 6121, Université de Provence-Aix-Marseille, Centre de Saint-Jérôme, 13397 Marseille Cedex 20, France.
* To whom correspondence should be addressed: e-mail P.V.Coveney@ucl.ac.uk.

10.1021/ma0503817 CCC: $30.25
Published on Web 06/16/2005

transform infrared (FTIR) spectroscopy has also been used to study the adsorption of low molecular weight amines by clays, for example, to demonstrate the presence of Brønsted acid sites in the clay interlayer.[13] However, these conventional analytical techniques are, by themselves, incapable of elucidating the interlayer arrangement, let alone the dynamical behavior, of the monomers in the organoclay composites. The computer simulation of models of experimental systems can be used to good effect to gain an understanding about the local arrangement and dynamics of intercalated organic molecules in clay−organic systems.[14−16]

In particular, molecular dynamics (MD) simulations allow the temporal evolution of a model system under near laboratory conditions (constant pressure and temperature) to be followed. The data from these simulations provide precise information regarding the coordinates of all atoms within the model at any point in time during the simulation period. This allows the interlayer arrangement and dynamics of organic and water molecules to be evaluated with equal precision.

There have been several MD simulation studies of the interlayer behavior and arrangement of quaternary alkylammonium species within clays. Zeng and co-workers, using a modified Dreiding force field, have shown that depending on the alkylammonium species used a range of interlayer arrangements including monolayers, bilayers, pseudo-trilayers, and pseudo-quadrilayers may be observed.[17,18] In an earlier study Pospíšil et al. examined the different intercalation behavior of ammonium surfactants in montmorillonite, paying particular attention to the host−guest interaction energies.[19] Heinz and co-workers have also examined the structural transitions in organoammonium clays where the ammonium has long alkyl chains, comparing simulation results with corresponding experimental measurements.[20,21] There has been very little work carried out where primary amine or ammonium intercalated clay systems have been addressed. Pospíšil et al. have carried out MD simulations on long chain alkylamine/ammonium intercalated clays. The aim of this study was to gain insight into the relative exfoliation energies of these organoclays.[22]

2. Primary Amine and Ammonium Species in Clays

In the preparation of clay−polymer nanocomposites it is often the case, depending on the method of synthesis, that the clay tactoids are almost fully separated (exfoliated) into individual clay sheets within the polymer matrix. It is desirable to be able to control the extent of exfoliation to produce composite materials with differing properties. For the oil field industry, the capability to suppress swelling and exfoliation in clayey deposits is vitally important to prevent degradation of oil bore holes.[4] Lin and co-workers have carried out a series of investigations into the behavior of primary amine intercalated clay compounds for these purposes.[23−27] These studies showed that di- and tri-primary amines can be acidified stepwise to give a controlled number of charged ammonium groups per monomer, which allows the cation exchange of the clay to be systematically varied and results in controlled modification of interlayer spacing.[23] Those primary amine/ammonium species with a hydrophobic backbone, e.g., poly(propylene oxide) (PPO), have a propensity to self-assemble within the clay interlayer, conferring well-controlled, defined interlayer separations (basal *d*-spacings). Depending on the molecular weight of the amine, the interlayer separation can vary from a monolayer to very large multilayer separations without exfoliation occurring and, in certain instances, unusual rodlike morphologies of the organoclay composite crystallites with long-range ordering.[24−26] The use of such amines offers a way to control the extent of exfoliation. Additionally, the use of different backbone lengths and compositions was observed to affect the amphiphilic properties of the clay−amine composites, resulting in a tunable solvophilicity that allows the clay particles to be dispersed in a variety of solvents for the preparation of clay−polymer nanocomposites.[27,28]

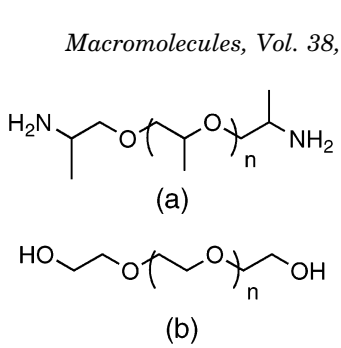

Figure 1. Structure of (a) poly(propylene oxide) bis(2-aminopropyl ether) (PPO-NH_2), molecular weight (M_w) 230 g mol^{-1} and, (b) poly(ethylene glycol) (PEG), M_w 400 g mol^{-1}, used in the preparation of organoclay composites.

We have previously reported the formation of montmorillonite composites with poly(propylene glycol) bis(2-aminopropyl ether) (PPO-NH_2) (Figure 1) intercalated between the clay sheets.[16] In the present paper we expand upon that work. These intercalated composites unfailingly form monolayered composites, in contrast with a wide range of other functionalized poly(alkylene oxides) of similar molecular weight that form bilayers in, and cause some degree of exfoliation of, the clay interlayer. The PPO-NH_2 composites also tend to be much more resistant to mechanical crushing (using a simple manual test) than any of the composites formed using the various other functionalized poly(alkylene oxide) monomers we studied.[15,16]

Lin and co-workers[24,29] and Xiao et al.[30] have postulated a variety of conceptual interlayer arrangements and interactions in an attempt to account for the observed interlayer separations in the amine−clay composites. We have speculated that the increased crush resistance of the amine composites, and the restricted interlayer spacing when low-M_w PPO-amines are used, results from specific hydrogen bonding arising between the amine/ammonium N−H groups and interlayer water and/or siloxane surface oxygen atoms on the silicate sheets, which is not possible in tertiary ammonium species.[16]

The purpose of the present paper is to report further investigations of the intercalation of low molecular weight unmodified poly(alkylene oxide) amines (Figure 1) into clays using a combination of experimental and computational studies, with composites analyzed by PXRD, TGA, and FTIR spectroscopy. One aim of the investigation is to elucidate whether the amine in solution is intercalated unaltered or as the protonated ammonium form and the effect this has on interlayer hydrogen bonding. In particular, we make use of the N−H bending absorption in the FTIR spectra of the composites, coupled with the absolute control of computer simulation, to elucidate the arrangement of interlayer anions and bonding patterns. Recently, Pironon

et al. have characterized clays containing NH_4^+ cations in some detail using FTIR spectroscopy.[31] In the next section the experimental and computational methods are described. This is followed in section 4 by a presentation of our results and a discussion bringing together the computer simulations and experimental observations. Finally in section 5, we draw conclusions regarding the nature of the monomer arrangements and the interactions in the interlayer region.

3. Methodology

In this section we discuss the techniques used to synthesize the organoclay nanocomposites and subsequently characterize the prepared materials. Computer simulation is used to interpret the observed experimental results. The organic and water contents of the models are based on the experimental structures.

3.1. Experimental Synthesis and Characterization of Organoclay Products. Poly(propylene oxide) bis(2-aminopropyl ether) with M_w 230 g mol^{-1} (PPO-NH_2) and poly(ethylene glycol) with M_w 400 g mol^{-1} (PEG) were purchased from Aldrich and used without further purification. For comparison, as a standard for FTIR, poly(propylene oxide) bis(2-(ammonium chloride) propyl ether) (PPO-NH_3Cl) was prepared by protonating PPO-NH_2 by the addition of 10% HCl solution. FTIR confirmed complete conversion of amine to ammonium salt ($-NH_3^+$ bending modes: 1608, 1508 cm^{-1} (cf. 1671, 1593 cm^{-1} for PPO-NH_2)). Montmorillonite clay was purchased from the Southern Clay Repository at Purdue University. The organoclay was prepared by stirring the clay (0.4 g) for an hour in water and then sonicating for a further 30 min to form a suspension. This was followed by addition of the organic compound (80 wt %), and the resulting suspension was sonicated for an additional 30 min. Excess water was removed by evaporation through placing the samples in an oven (ca. 80 °C) overnight.

Four experiments were performed: (i) the intercalation of PPO-NH_2 vs PEG in Na^+-montmorillonite; (ii) the intercalation of PPO-NH_2 in Na^+-montmorillonite; (iii) the intercalation of PPO-NH_3 in Na^+-montmorillonite; (iv) intercalation of a PPO-NH_2/PPO-NH_3 mixture in Na^+-montmorillonite. The resulting organoclays were characterized by a variety of techniques. X-ray diffraction (XRD) measurements were carried out on a Siemens d5000 diffractometer. Powder samples were either mounted on a silicon wafer (v20 slits) or as a bulk powder (v6 slits). Scans were from $2\theta = 2.5-15°$, in steps of 0.020° with a time step of 2.5 s. The X-ray generator was operated at 40 kV and 40 mA. Fourier transform infrared (FTIR) measurements were carried out on a Perkin-Elmer 1600 series FTIR instrument, using a KBr disk, scanning from 4000 to 400 cm^{-1}, with 16 scans recorded for each run. Thermogravimetric analysis (TGA) was performed on a Perkin-Elmer Pyris 1, scanning from room temperature to 600 °C at 10 °C/min.

3.2. Computer Simulation of Organoclays. The model clay−polymer systems were prepared as described in our previous work in this area.[15,16] The molecular dynamics simulations were performed using LAMMPS (large-scale atomic/molecular massively parallel simulator).[32,33] LAMMPS uses algorithms and techniques, such as spatial domain decomposition (where the system is spatially decomposed into subdomains that are then distributed across the processors), that allow the code to exhibit a near linear relationship (scaling) between the number of processors used, or the size of the model system of interest, and the time taken for the simulation to be performed.[34,35] For added efficiency, the calculation of the computationally demanding long-range electrostatic interactions is carried out using the particle−particle particle−mesh algorithm (PPPM)[36−39] and time-stepping performed using the rRESPA integrator,[40] which is a multiple time-stepping algorithm.

To model the bonded and nonbonded interactions, the Teppen force field, an extension of the consistent force field (cff91) force field which has been specifically parametrized to account for the behavior of clay minerals, as well as describing the organic molecules, was used for the simulations.[34,41,42] The Teppen force field is a type II force field that contains cross-terms (bond−bond, angle−angle, mid-bond torsion, and end-bond torsion, for instance) in addition to the usual two-body, three-body, and four-body terms. Short-range nonbonded interactions are described using a Lennard-Jones 9−6 potential. Hydrogen bond donor and acceptor atom interactions are not explicitly described within the force field. This force field has already been validated for the swelling behavior of the Na^+-montmorillonite clay[35] and used to study the interlayer arrangement and dynamics of clay−polymer nanocomposites.[15,16,43]

To correlate with our experimental investigation, and since it was not possible to determine accurately the amount of Na^+ exchanged from the clay, results from simulation studies of four possible scenarios, using experimental loadings of organic material and water, are also reported: (i) none of the Na^+ was exchanged and all the amine was unprotonated ($-NH_2$); (ii) 33% of the ($-NH_2$) and Na^+ was exchanged by ammonium species ($-NH_3^+$); (iii) 66% of the Na^+ was exchanged by ammonium species and all the monomer was protonated ammonium ($-NH_3^+$); (iv) equivalent to exchange of 83% of the Na^+ cations.

The procedure by which the model organic molecules, clay, and clay composite were generated in our simulations is described in detail in Boulet et al.[15] The model clay unit cell used was a Wyoming-like montmorillonite with stoichiometry $[Al_{60}Mg_8]$ $[Si_{128}O_{384}H_{64}]Na_{12}$. The octahedral layer of the clay unit cell had 8 Mg atoms (negatively charged sites) for every 56 Al atoms, while each of the two tetrahedral silicate layers contained 2 Al substitutions for every 62 Si atoms. A set of low-energy conformers of PPO-NH_2 monomers was generated using Monte Carlo sampling. The PPO-NH_2 conformer with the highest radius of gyration (most linear) was inserted into the interlayer of the clay unit cell, along with water molecules, using a canonical Monte Carlo simulation to give models with the experimental loading. This PPO-NH_2 model was energy-minimized and run for a short (50 ps) period of molecular dynamics (MD) simulation. The $-NH_2$ groups in the final model were modified to $-NH_3^+$ groups and Na^+ cations removed to generate the four systems described above; the new models were again energy minimized and run for 50 ps of MD simulation. The resulting models were subsequently replicated to create the supercells used to generate the results described in this study. The supercell composition of each model system is given in Table 1.

In this study we restricted our initial simulations to models with two interlayer spaces and 7160 atoms (i.e., a $2 \times 2 \times 2$ array of clay unit cells), and the systems were simulated for 1 ns at 300 K using an isobaric−isothermal (NPT) ensemble in which the temperature

Table 1. Simulation Cell Compositions of Modeled Clay−Amine Systems[a]

monomer	no. of species: water	no. of species: end group	no. of species: Na^+	time run (ns)	atom no.	supercell size/Å
PPO-NH_2	56	80	96	1.8	7160	41 × 71 × 27
PPO-NH_3^+	56	80	16	1.0	7160	41 × 71 × 28
PPO-NH_2/-NH_3^+	56	16/64	32	1.0	7160	41 × 71 × 30
PPO-NH_2/-NH_3^+	56	48/32	64	1.0	7160	41 × 71 × 27
PPO-NH_3^+	294	3920	784	0.5	350840	284 × 497 × 28

[a] The number of monomers and water in the interlayer was constant, based upon the experimental TGA data for the PPO−NH_2 system, and corresponded to 10% mass organic content and 1% mass water.

was controlled via a Langevin thermostat. Two interlayer spaces were used in order to remove artificial features within the clay sheet associated with periodic effects when using just one interlayer space. One of the initial models was run for a further 0.8 ns to examine the effect that run time had on the data produced. To investigate finite size effects, one of the initial models was further replicated to form a supercell containing around 350 000 atoms, which was then run for 0.5 ns. This vastly increased model size exploits the ability of the LAMMPS code to scale linearly where the number of atoms: the processor ratio is kept at unity; i.e., 2000 atoms on two processors will take the same time to run as 1000 atoms on one processor.[32] The maximum number of processors available to us was 256, so for a 0.5 ns run we could build a model approximately 64 times as large (256/(8 × 0.5)) as the 7160-atom model and keep the same wall clock simulation time. Allowing for some falloff in the scaling from ideal linear performance, we decided to build a model 49 times as large as the 7160-atom model, and a 7 × 7 replication of the 7160-atom super cell gave a new supercell of 350 840 atoms.

Three-dimensional periodic boundary conditions were applied to compute the electrostatic interactions by Ewald summation and to represent the bulk material. Data were collected every 100 ps, and statistical averages were evaluated over the last 800 ps of simulation. Each 7160-atom molecular dynamics simulation, with a total simulation time of 1 ns, took ≈45 h of real "wall clock" time on eight processors of the SGI Origin 3000 supercomputer "Green" at CSAR, Manchester. The 350 000-atom large-scale simulation was run for 0.5 ns and took ca. 83 h on 128 processors of Green.

Analysis of the potential energy of each simulation showed that all of the 7160-atom model systems, as well as the 350 000-atom model, were equilibrated within the first 0.2 ns of simulation, and data collection was started after this period. The remaining simulation time was used for data analysis. Time-averaged radial distribution functions (RDFs) and one-dimensional atom distribution maps were calculated for selected atom types. The environment about the defined atom type was analyzed using RDFs, which show the distribution of an atom type with respect to a defined atom type, normalized to a totally random distribution. The one-dimensional atom density maps, which represent the distribution of atoms in the interlayer taken as a slice through the *ac* crystallographic plane of the clay interlayer, were averaged along the *bc* crystallographic plane and over the simulation data collection time period. The 7160-atom models were visualized on an Apple Macintosh G4 PowerBook using the UCSF Chimera package.[44] The 350 000-atom model was visualized using the Atom Eye software package, which has more efficient rendering capabilities for larger systems.[45]

Table 2. Effect of Solution Organoamine Concentration upon *d*-Spacing and Monomer Loading in Na^+-Montmorillonite

poly(alkylene oxide)	wt % (based on clay)	wt % (based on total)	*d*-spacing/Å
PPO-NH_2	160	62	13.5
PPO-NH_2	80	44	13.7
PPO-NH_2	40	30	14.3
PPO-NH_2	13	12	13.6
PPO-NH_2	7	6	13.8
PEG-400	70	41	17.7
PEG-400	40	30	17.5
PEG-400	14	13	17/13
PEG-400	11	10	13.7
PEG-400	7	7	13.2

4. Results and Discussion

In this section we first confirm through experiment and modeling the findings of previous reports that intercalation of PPO-NH_2 is hindered, and only an interlayer spacing conforming to a monolayer is observed irrespective of initial solution concentration, while low molecular weight PEG is intercalated in increasing amounts until an interlayer spacing corresponding to a bilayer is formed. In the subsequent sections the interlayer arrangement and bonding in the PPO-NH_2 monolayer systems are investigated.

4.1. Intercalation of PPO-NH_2 vs PEG. Table 2 shows data for various concentrations of added organoamine species. The PPO-NH_2 organoclay results only show *d*-spacings corresponding to monolayer formation (ca. 14Å), even at very high initial solution concentrations of the PPO-NH_2. This is in contrast to PEG, which shows the presence of a *d*-spacing of ca. 17 Å, indicating bilayer formation even at relatively low solution concentrations of 14% weight monomer (based on clay). Chou et al., who studied experimentally the uptake of the ammonium salt of PPO-NH_2 of M_w 230, predicted bilayer formation based on the cation exchange capacity of the clay but in fact observed a monolayer with an interlayer separation of ca. 15 Å irrespective of the initial concentration of amine used.[25] The authors suggested that this was due to incomplete cation exchange by the amine. We also find that, even if all the PPO-NH_2 is protonated, the experimental interlayer organic content only corresponds to 82% cation exchange in our model clay systems (Table 1).

Lin and co-workers postulated that the Na^+ cations limit the amount of monomer intercalated, either through the cation exchange capacity or by providing attractive positive electrostatic sites for the backbone oxygen atoms. However, as the low molecular weight PEG system does swell, it seems likely that the difference in backbone chain between PPO and PEG must have a determining influence.[25,29]

This raises questions about the factors determining the amount of organic material that can intercalate into

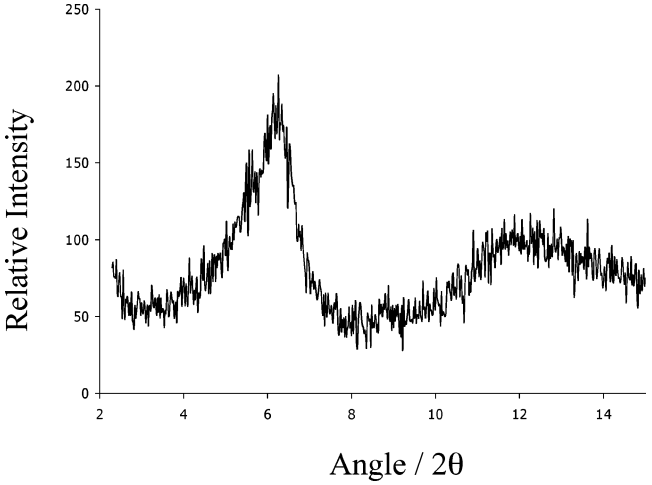

Figure 2. X-ray powder diffraction pattern for the poly(propylene oxide) diamine Na^+-montmorillonite nanocomposite material. The PPO-NH_3^+ and mixed PPO-NH_2/PPO-NH_3^+ composites have near identical XRD patterns to this one.

clay composite materials and the effect that this has on interlayer separations. We have previously reported that the amount of water, type of cation, and monomer functional headgroup all interact in a subtle way to determine interlayer arrangements.[15,16] Having established that the PPO-NH_2 system only formed a monolayer, the next stage in this work was to investigate the nature of the interactions between the amine and the clay sheets.

4.2. Interlayer Arrangement and Bonding in PPO-NH_2 Organoclays. *Experimental Results.* The basal reflection region of the powder XRD pattern of the PPO-NH_2 composite is shown in Figure 2 and has a *d*-spacing of 14.3 Å. Though the two characteristic FTIR primary amine N−H stretching modes (above 3000 cm^{-1}) were observed in the amines without clay, upon intercalation this region was overlaid with complex O−H stretch absorptions from the clay hydroxyl groups and interlayer water such that no useful information could be gleaned. The primary amine N−H bond bending region (1640−1560 cm^{-1}) proved more useful for analysis. The FTIR spectrum of PPO-NH_2 in the absence of clay (Figure 3c) shows NH_2 bending mode absorptions at 1593 cm^{-1} (with a shoulder at 1671 cm^{-1}) and characteristic N−H stretching frequencies of 3290 and 3367 cm^{-1}. The high frequencies of the N−H bending mode are indicative of N−H· · ·N hydrogen (H-) bonding in the free PPO-NH_2.

Figure 3d shows that, upon intercalation of PPO-NH_2 into the montmorillonite interlayer, the FTIR spectrum changed, with two distinct NH_2 bending mode absorptions observed, one at 1640 cm^{-1} and the other at 1576 cm^{-1} (Table 3). The absorption at 1640 cm^{-1} is of high frequency relative to the principal absorption in the unintercalated PPO-NH_2 at 1593 cm^{-1} and suggests substantial H-bonding is occurring in the montmorillonite PPO-NH_2. This change in N−H bending absorption frequency in the intercalated PPO-NH_2 relative to free PPO-NH_2 is typical of clay−amine interactions, indicating that some of the PPO-NH_2 is intercalated as the unprotonated $-NH_2$ species.[46] Over a more prolonged heating period (up to 9 days at 80 °C) the absorption at 1576 cm^{-1} is reduced in intensity compared to the 1641 cm^{-1} absorption, which also shifts to a slightly higher frequency (1656/8 cm^{-1}) and broadens.

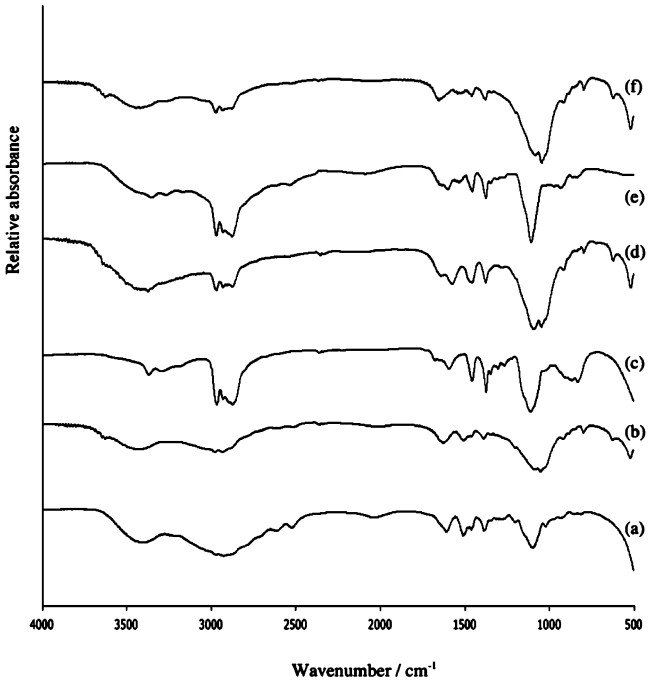

Figure 3. FTIR spectra of (a) free poly(propylene oxide) diammonium (PPO-NH_3^+) and (b) intercalated in Na^+-montmorillonite; (c) free poly(propylene oxide) diamine (PPO-NH_2) and (d) intercalated in Na^+-montmorillonite; (e) free poly(propylene oxide) diamine/ammonium mix (PPO-NH_2/PPO-NH_3^+) and (f) intercalated in Na^+-montmorillonite.

The FTIR studies suggest that a significant fraction of the PPO-NH_2 amine groups remain unprotonated within the clay interlayer, and the principal absorption band observed in the FTIR spectra of the PPO-NH_2 composite arises due to interactions between the amine groups and the interlayer water and cations and/or the siloxane surface oxygen atoms of the clay sheets. The nature of this bonding is investigated in more detail below with the aid of molecular modeling.

Simulation Results. The PPO-NH_2 molecules in the simulated 7160-atom PPO-NH_2 composite formed a monolayer with a *d*-spacing of 13.98 ± 0.002 Å. This is in good agreement with the experimental value of 14.3 Å. Figure 4j−l shows the atom density distribution across the interlayer regions. The PPO-NH_2 N atoms are located slightly offset either side of the midplane of the interlayer. Little or no H-bonding occurs between the amine groups and the siloxane surface oxygen atoms in the tetrahedral layer of the clay sheet. The other atoms in the PPO backbone are observed to lie along the midplane of the interlayer region.

The water molecules in the PPO-NH_2 composites are arranged almost parallel with the clay sheets, the water O atoms being arranged near the interlayer midplane, but oriented toward the face of the clay sheets with the water H atoms residing close to, but slightly offset from, the midplane of the interlayer. As in all the systems we have investigated, Na^+ cations were arranged mainly adjacent to the face of the clay sheet, sometimes penetrating into the tetrahedral layer slightly.

The radial distribution function (RDF) for the PPO-NH_2 composite (Figure 5) shows that the Na^+ cations are closely coordinated by the O atoms of the PPO backbone (2.6 Å), the interlayer water (2.4 Å), and the clay sheet (2.6 Å) but also by the N atoms of the amine groups (2.5 Å). A PPO-amido-sodium cation coordination has also been postulated by Lin et al., who suggested

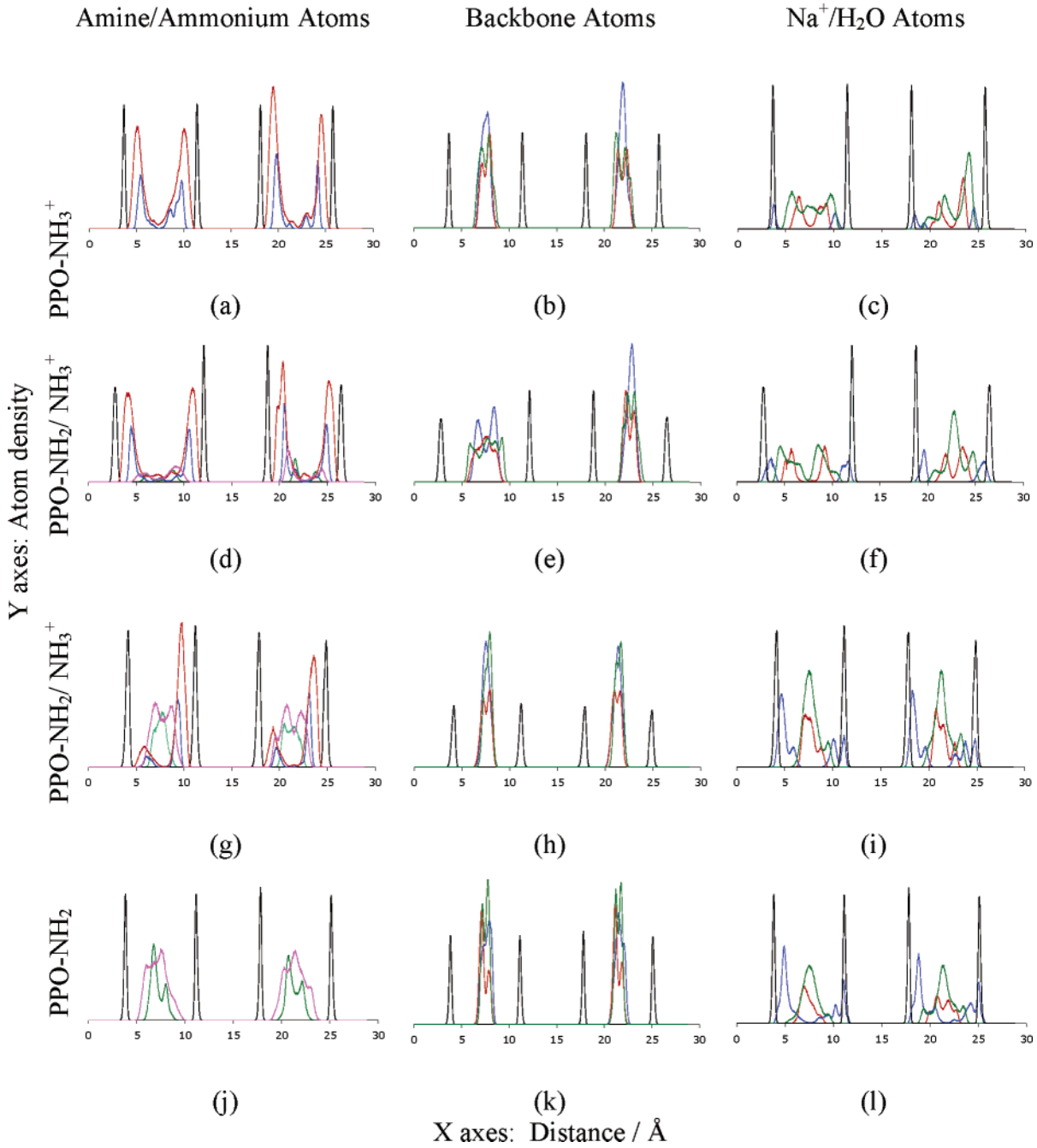

Figure 4. One-dimensional atom density maps for interlayer species in MD simulations of (a−c) poly(propylene oxide) diammonium ($PPO\text{-}NH_3^+$); (d−f) poly(propylene oxide) 20% diamine/80% ammonium mix ($PPO\text{-}NH_2/PPO\text{-}NH_3^+$); (g−i) poly(propylene oxide) 60% diamine/40% ammonium mix ($PPO\text{-}NH_2/PPO\text{-}NH_3^+$); (j−l) poly(propylene oxide) diamine ($PPO\text{-}NH_2$) Na^+-montmorillonite composites. Atom types shown are (a, d, g, j) interlayer amine/ammonium groups where siloxane surface clay O atoms are black, ammonium N are blue, ammonium H are red, amine N are green, amine H are pink; (b, e, h, k) interlayer PPO backbone atoms where **C**−O are blue, **O**−C are red, C methyl are green; (c, f, i, l) interlayer water and Na^+ where Na^+ are blue, water O are red, and water H are green.

Table 3. Observed FTIR N−H Bending Mode Absorption Peaks for Various Amines and the Corresponding Na^+-Montmorillonite (Na-Mmt) Composites

	N−H bend FTIR absorptions/cm^{-1}			
intercalant	no clay	Na-Mmt aged 1 day	Na-Mmt aged 5 days	Na-Mmt aged 9 days
$PPO\text{−}NH_2$	1671/1593	1640/1576	1656/1560	1658/1561
$PPO\text{−}NH_3Cl$	1608/1506	1622/1507	1631/1505	1621/1503
$PPO\text{−}NH_2/PPO\text{−}NH_3Cl$	1643/1600/1547/1537	1652/1558	1658/1559[a]	

[a] Sample aged for 4 days.

that the combined O and N atom coordination to Na^+ provide a driving force for adsorption of the organic molecules.[29]

The effects of allowing simulations of this model system to run for longer for a further 0.8 ns were also considered. For example, the 1-d atom density plots for

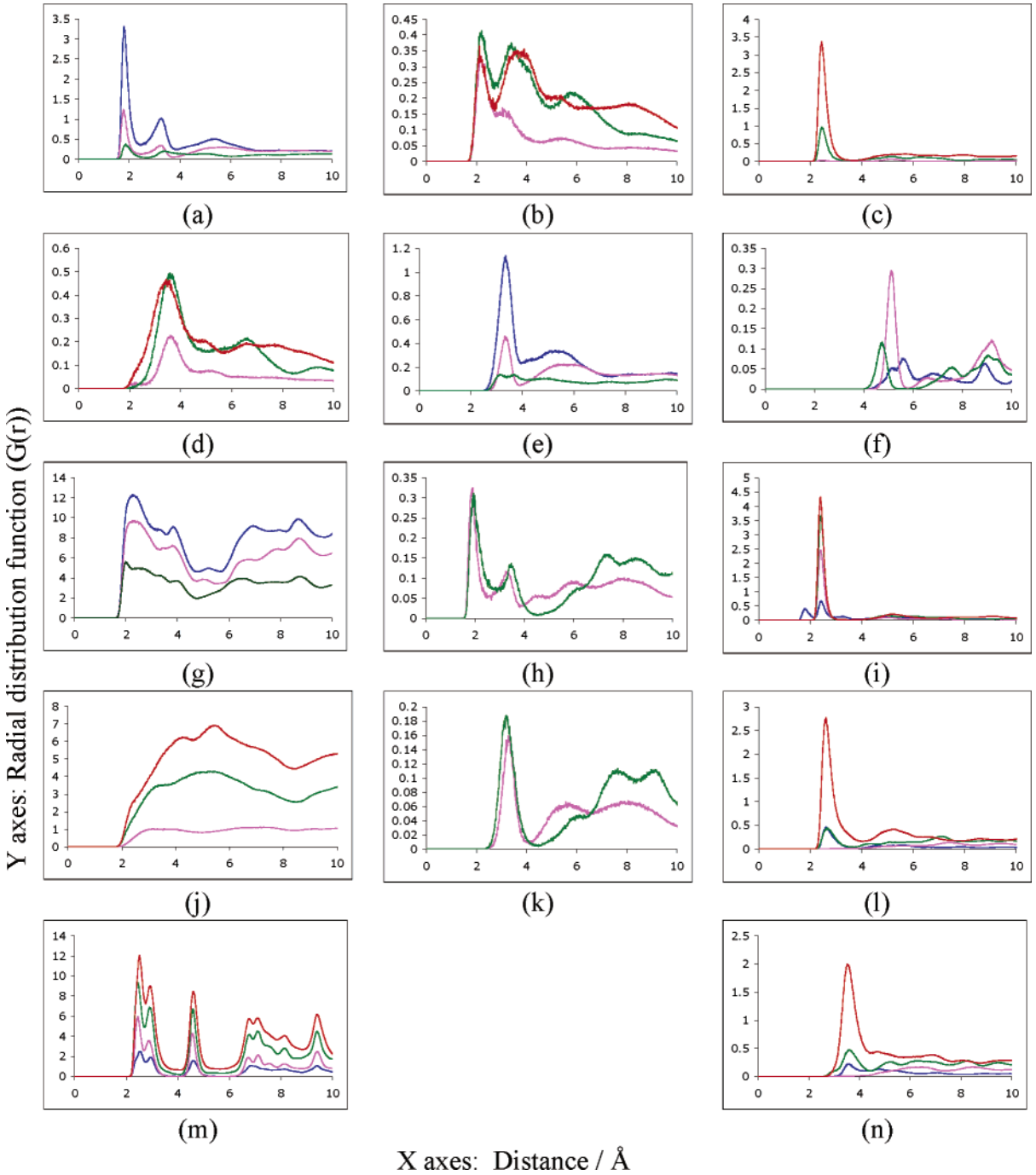

Figure 5. Radial distribution functions for simulated ca. 10K atom models between (a) ammonium H and water O, (b) amine N and water H, (c) Na^+ and amine N, (d) amine H and water O, (e) ammonium N and water H, (f) Na^+ and ammonium N, (g) ammonium H and siloxane surface clay O, (h) amine N and ammonium H, (i) Na^+ and water O, (j) amine H and clay siloxane surface O, (k) ammonium N and amine H, (l) Na^+ and PPO O, (m) Na^+ and siloxane surface clay O, (n) Na^+ and PPO methyl C atoms. PPO$-NH_3^+$ are blue, 20% diamine/80% ammonium mix (PPO-NH_2/PPO-NH_3^+) are pink, 60% diamine/40% ammonium mix (PPO-NH_2/PPO-NH_3^+) are green, and PPO-NH_2 are red.

the amine N atoms and the RDF of the amine N atom distribution around the Na^+ cations for this system over 100 ps intervals finishing at 0.3, 1.0, and 1.8 ns were examined. Though the RDF change only slightly over the 1.8 ns simulation period, the amine N atom distribution in one of the interlayer regions moved from an initially asymmetric to an equal distribution either side of the midplane of the interlayer region.

4.3. Interlayer Arrangement and Bonding in PPO-NH_3^+ Organoclays. *Experimental Results.* The observed interlayer spacing for the PPO-NH_3^+ composite is 14 Å, which corresponds to a monolayer of organic molecules in the clay interlayer, as does the results of Lin and Chen, who reported a basal spacing of 15 Å.[28] The small difference in interlayer spacing between the two results is most likely due to slight differences in the clay and preparatory procedure used.[28] By comparison to nonintercalated PPO-NH_3Cl, which showed N−H bend absorptions at 1608 and 1506 cm^{-1}, the FTIR spectra of the PPO-NH_3Cl composite (Figure 3a) showed absorptions at 1623 and 1507 cm^{-1}, which remained nearly unchanged for composites dried in the oven for up to 9 days (Table 3). This shift to higher frequencies upon intercalation suggests an increase in hydrogen-

bonding (H-bonding) interactions commensurate with the creation of interactions between the ammonium H atoms and the siloxane surface oxygen atoms of the aluminosilicate clay layer. Additional H-bonds are also likely to exist between the ammonium group and interlayer water.[47]

Simulation Results. The simulated *d*-spacing for the 7160-atom system ammonium composite was 14.39 Å (with a standard deviation of ±0.001 Å), in reasonable agreement with the experimental work of both ourselves and others,[28] but ≈0.5 Å more than for the simulated PPO-NH_2 composite.

The reason for this difference can be found by considering the atom distribution within the interlayer (Figure 4a−c) and comparing it to the distribution for the PPO-NH_2 model (Figure 4j−l). Figure 4a shows the distribution of the ammonium group N and H atoms in comparison to the siloxane surface O atoms of each clay layer. The ammonium groups are predominantly arranged adjacent to the face of the clay sheets, with the ammonium H atom density closer (ca. 1.5 Å) to the siloxane surface O atoms than the ammonium N atom density (ca. 1.9 Å), indicating the formation of a domain of ammonium groups H-bonded to the aluminosilicate sheets. The slightly expanded interlayer in the PPO-NH_3^+ composite arises due to conformational changes in the molecules, discussed in the next paragraph, to allow the positively charged ammonium (−NH_3^+) groups to locate adjacent to the negatively charged clay sheets, which also increases H-bonding interactions between the ammonium H atoms and the O atoms of the silicate sheet. This conformational change does not occur when only uncharged amine (−NH_2) groups are present.

The PPO-NH_3^+ backbone C and O atoms (Figure 4b) are arranged along the midplane of the interlayer region, with the methyl groups and the O atoms both slightly offset either side of the midplane, due to the staggered nature of these groups in the PPO backbone. This arrangement of the poly(propylene oxide) backbone contrasts with that observed in monomers with poly(ethylene oxide) backbones studied previously by ourselves, which preferred an arrangement whereby the backbone C and O atoms lay adjacent to the clay sheet.[16]

The Na^+ cations adopted positions along the face of the clay sheets (Figure 4c), in some cases interpenetrating the rings formed by the siloxane surface oxygen atoms of the tetrahedral aluminosilicate layer, as we have previously found.[16] In the case of the ammonium-intercalated composites with very few Na^+ cations the interlayer water adopted an arrangement close to the faces of the clay sheets, with the water H atoms oriented predominantly closer to the face of the clay sheet than the water O atoms. This arrangement of water molecules is in contradistinction to the PPO-NH_2 composites where the water O atoms were arranged near to the interlayer midplane and oriented coplanar with the clay sheets.

A more detailed analysis of the local environment about each atom type is given by the RDFs in Figure 5. It can be seen that the ammonium cation H atoms are coordinated strongly by interlayer water (1.8 Å internuclear separation, Figure 5a), indicating that the ammonium ion behaves somewhat akin to a Na^+ cation (Figure 5i). The ammonium H atoms also strongly interact with the siloxane surface O atoms of the clay sheet (Figure 5g) at a distance of some 2.4 Å, as suggested by the 1-d atom distributions. This arrangement of the positively charged ammonium groups is again similar to the similarly charged Na^+ cations, shown in Figure 5m (main peak at 2.6 Å internuclear separation), which also interact closely with the O atoms in the PPO backbone (Figure 5o). The nature of the interaction of the ammonium cations with the clay sheets is illustrated in Figure 6a: the ammonium group is oriented such that the H-bonding and favorable electrostatic interactions are maximized. In conditions of low interlayer water content, Na^+ cations, by comparison, tend to interpenetrate slightly into cavities within the tetrahedral layer of the clay sheet (Figure 6b) so as to maintain a full coordination shell of O atoms made up partly by water, partly by clay.

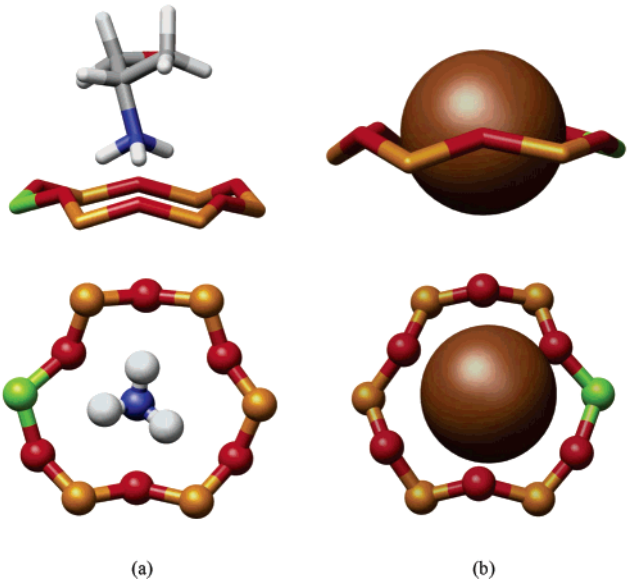

Figure 6. Snapshots after 1 ns of molecular dynamics simulation of the 7160-atom 60% diamine/40% ammonium mix (PPO-NH_2/PPO-NH_3^+) system showing (a) the interlayer arrangement of ammonium cations and adjacent clay sheet atoms (other atoms omitted for clarity). The ammonium cation is arranged to maximize H-bond and electrostatic interactions. When compared to the Na^+ cation, (b) the ammonium cation is unable to sit closer to the cavities in the tetrahedral layer of the clay sheet due to steric restrictions and strong H-bond interactions with surface siloxane surface O atoms. The color scheme is C gray, H white, O red, N blue, Si orange, Al green, and Na^+ brown.

The large-scale, 350 840-atom system run for 0.5 ns showed an average simulated *d*-spacing of 14.40 ± 0.001 Å. The 1d-atom maps were found to differ from the corresponding 7160-atom model (Figure 7a): the distribution of atom types retained the same broad features in both model systems, but the atom density in the system with 350 840 atoms was found to be less constrained than in the smaller model. Visualization reveals the existence of long wavelength undulations in the clay layers (Figure 8). It is likely that this effect is due to the exceptionally large supercell employed; small periodic models are much more tightly constrained by symmetry to rigid clay sheets. In short, the absence of such undulations is due to finite size effects. The observation of such clay sheet undulations is of significance as they could feasibly allow the calculation of certain materials properties, for example tactoid elasticity, which are otherwise hard to obtain. Similar finite size effects have been reported previously in atomistic simulations of biological membranes.[48] We plan to return with a more detailed study of these undulations in future work.

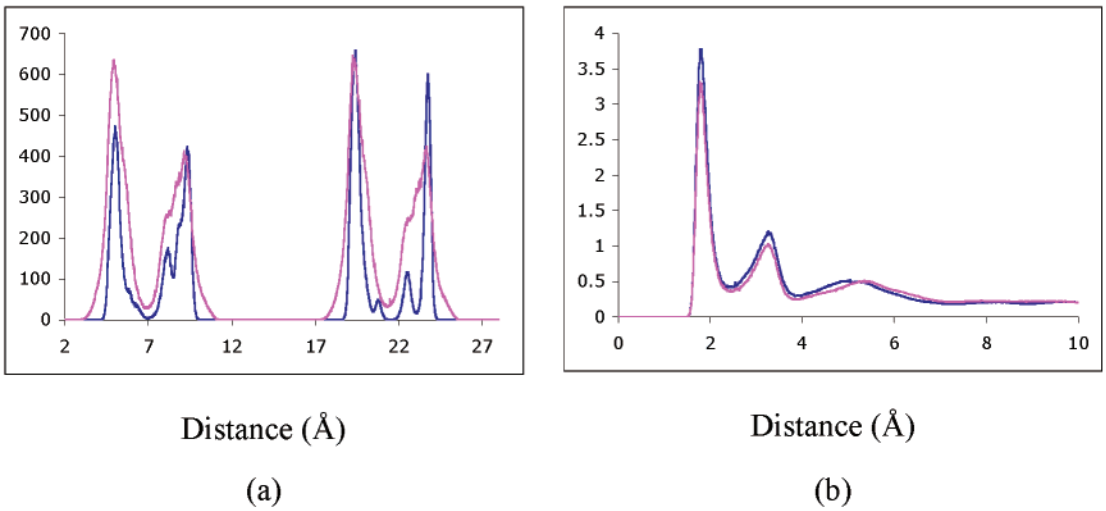

Figure 7. Effect of increasing the simulation cell size from 7160 atoms (blue line) to 350 840 atoms (pink line) on the evolution of the PPO-NH_3^+ model system, using the 1-d density map (averaged over 500 ps) for the amine N atoms (a) and the RDF (averaged over 500 ps) between the ammonium H atoms and the water O atoms (b).

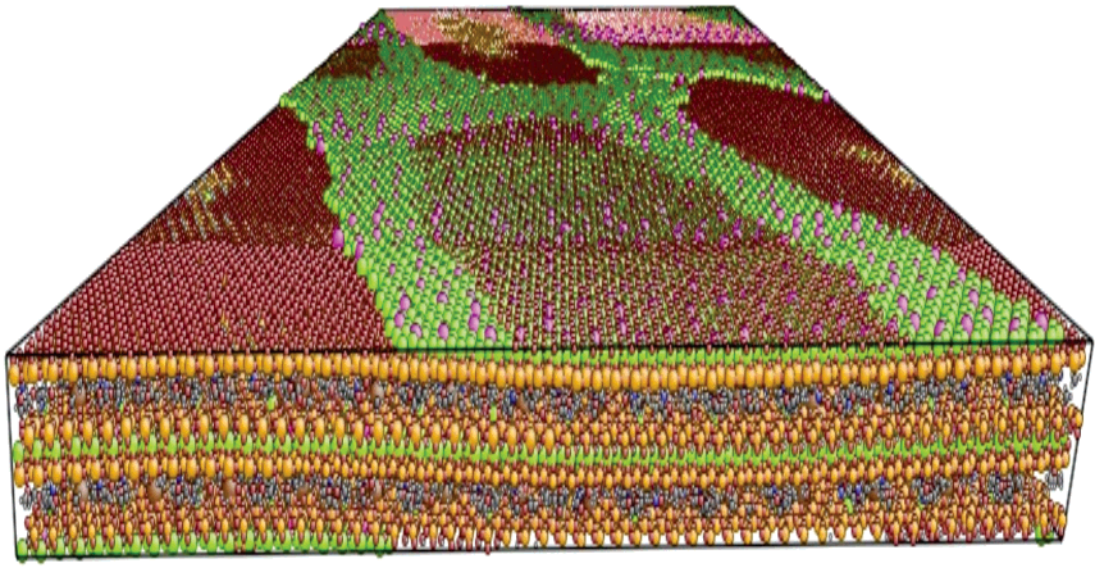

Figure 8. Snapshot of the 350 840-atom supercell after 0.5 ns of MD simulation showing a perspective view of the rectilinear supercell, the clay sheets exhibiting gentle undulations. The vertical scale is exaggerated to facilitate visualization of the undulations. The upper-most face of the periodic simulation cell shows the effect of the undulations with the clay Al and Mg octahedral layer being visible in some areas but not in others, according to where the periodic boundary bisects the waveform of the undulation. The color scheme is C gray, H white, O red, N blue, Si orange, Al green, Mg magenta, and Na brown. Periodic boundary conditions are imposed in all three orthogonal space directions. The image was rendered using Atom Eye software.

4.4. Interlayer Arrangement and Bonding in PPO-NH_3^+/PPO-NH_2 Organoclays. *Experimental Results.* Without the clay, multiple absorptions were observed in the N−H bending region within the FTIR spectra of the mixture (Table 3), indicating that a range of N−H environments are present. The characteristic doublet in the N−H stretching region (3266 and 3353 cm^{-1}) indicated the continuing presence of PPO-NH_2 in the mixed PPO-NH_2/-NH_3^+ solution. The principal N−H bending mode absorption peaks of the PPO-NH_2/-NH_3^+ composites were similar to those observed in the dried PPO-NH_2 composites (Table 3). Table 3 also shows that negligible changes were observed to the PPO-NH_2/-NH_3^+ composite FTIR spectra after heating the sample in the oven at 80 °C for 5 days. In the PPO-NH_2/-NH_3^+ mixture, a N−H bending absorption was observed at 1559 cm^{-1}, at higher wavenumbers than any adsorption observed in the composites prepared using wholly PPO-NH_3Cl (highest N−H bending absorption observed at 1631 cm^{-1}). The presence of the higher wavenumber N−H bending absorptions in the PPO-NH_2/-NH_3^+ solution and composite, but not in the PPO-NH_3Cl composites, suggests that the 1658 cm^{-1} absorption observed in the PPO-NH_2 composite is due to strong H-bonding arising between intercalated PPO-NH_2 and formed PPO-NH_3^+ species.

Simulation Results. The simulated PPO-NH_3^+/NH_2 composites had average *d*-spacings of 13.69 ± 0.001 Å and 15.15 ± 0.001 Å for the 40% ammonium:60% amine and the 80% ammonium:20% amine systems, respectively. The larger average *d*-spacing for the latter case arises due to one of the interlayers in the model unit cell being significantly more expanded (ca. 15.9 Å) than the other (ca. 14.4 Å), the reason for which is described in more detail below.

An examination of the atom density distribution across the interlayer shows that the ammonium groups in both PPO-NH_3^+/NH_2 composites (Figure 4d,g) be-

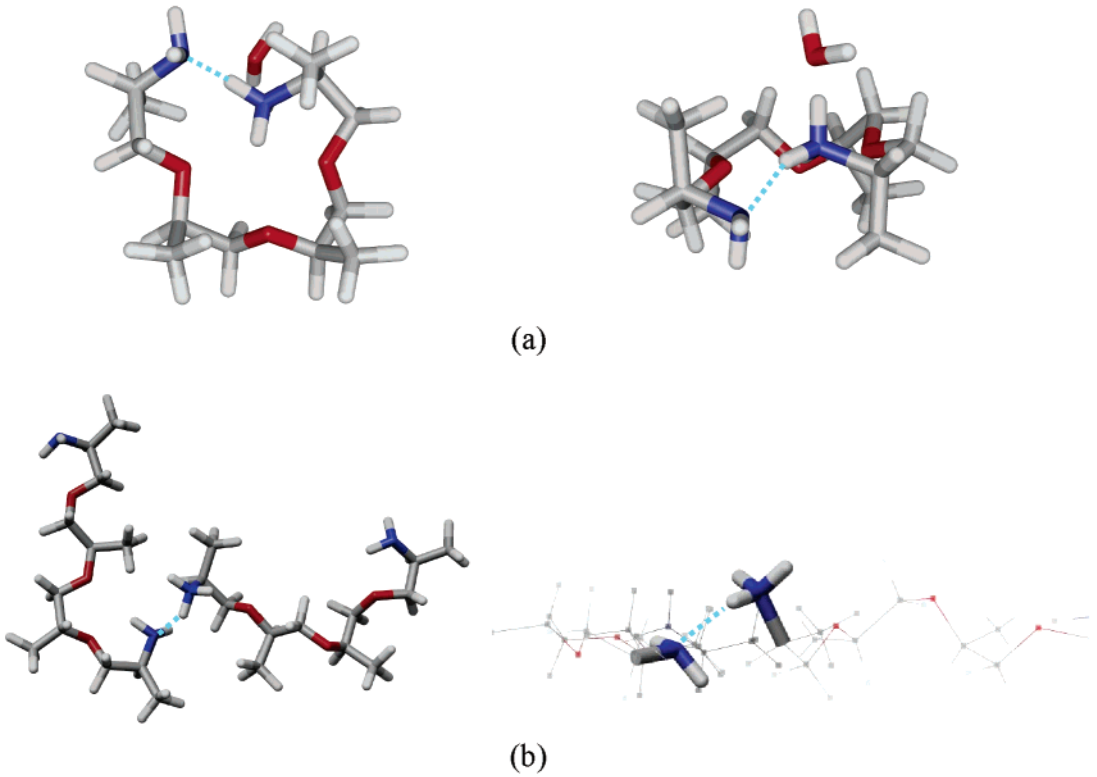

Figure 9. Snapshots taken after 1 ns of molecular dynamics simulation of the 7160-atom PPO-NH_2/NH_3^+ clay system showing (a) intramolecular H-bonding (N· · ·H distance = 1.740 Å) and (b) intermolecular H-bonding (N· · ·H distance = 1.936 Å); for clarity in left-hand image backbone atoms are in wire frame and have been clipped. Left-hand side images are viewed from perpendicular to the plane of the clay sheet, while right-hand side images are viewed parallel to the plane of the clay sheet. The color scheme is the same as for Figure 8, with H-bonds shown in pale blue.

haved similarly to those in the PPO-NH_3^+ composite (Figure 4a), being found adjacent to the clay sheet siloxane surface O atoms. In contrast to the PPO-NH_2 composite (Figure 4j), the amine groups in the 80% ammonium system were further away from the midplane of the interlayer, with the bulk of the amine H atom density located toward the positively charged ammonium groups (Figure 4d), suggesting possible H-bonding between these species, which is manifested in the RDF plot discussed later. The amine groups in the 40% ammonium system were distributed more in line with the amine groups in the PPO-NH_2 composite (Figure 4g). The monomer backbone carbon and oxygen atoms were distributed in the midplane of the interlayer (Figure 4e,h), with the exception of the much wider interlayer noted above, which we now address.

In this larger interlayer phase, of *d*-spacing ca. 16 Å, the poly(propylene oxide) C atoms appeared to form a bilayer, or pseudo-bilayer, arrangement as shown by the one-dimensional atom density in Figure 4e. The pendant methyl groups formed a pseudo-trilayer, and the O atoms were broadly distributed. Visualization of the monomers (Figure 9a) showed that this was due to intramolecular hydrogen-bonding causing a coiled monomer conformation to arise, resulting in an apparent bilayer arrangement.

The distributions of Na^+ cations and water across the interlayer are similar to those of the PPO-NH_3^+ composite (Figure 4c) for the 80% ammonium system (Figure 4f—excepting the pseudo-bilayer interlayer) and followed the PPO-NH_2 composite (Figure 4i) for the 40% ammonium system (Figure 4l). This illustrates that the distribution of interlayer Na^+ and water varies according to the number of amine groups that have been protonated. So far as the intercalated organic molecules are concerned, in scenarios where there are predominantly ammonium groups the interlayer adopts an arrangement similar to the case where there are all ammonium groups, and vice versa for amine groups and compounds.

The radial distribution functions for the amine N atoms (Figure 5h) show that the ammonium H atoms approach within 1.9 Å on average, indicating strong H-bonding. In Figure 9a the specific intramolecular H-bond (based on interaction distance criteria) shown has an N−H distance of 1.74 Å. It seems that this "proton sharing" results in there being little change in the FTIR spectra of the intercalated PPO-NH_3^+/NH_2 mixture relative to the solution phase PPO-NH_3^+/NH_2 mixture. The strong nature of such H-bonding in the simulated system would also be a plausible explanation for the high shift noted for the N−H bending mode absorption (indicative of H-bonding) in the PPO-NH_2 and PPO-NH_3^+/NH_2 composites FTIR spectra, suggesting that in the PPO-NH_2 composite a mixture of H-bonded $-NH_2$ and NH_3^+ groups exist in the interlayer, rather than just $-NH_2$. The use of atomistic methods prevents bond cleavage/formation and actual proton exchange occurring between amine and ammonium, although this could be investigated using ab initio methods.[49,50]

5. Conclusions

We have presented a combined experimental and computational study of the intercalation of some low molecular weight poly(propylene) oxide diamines within Na^+-montmorillonite. It has been confirmed that only a monolayer arrangement is observed upon intercalation

of PPO-NH_2, while a bilayer may be observed with PEO-NH_2. In contrast to other studies, we have rationalized the clay interlayer molecular arrangements and interactions using an FTIR analysis of N−H bending modes and extensive molecular simulation.

The interlayer spacing under the controlled conditions of computer simulations, for systems that only differ in the number of amine/ammonium groups and Na^+ cations, was found to be dependent on the number of intercalated ammonium groups and showed good agreement with the experimentally observed monolayers at similar organic and water loadings. Computer simulation shows that the organic molecules studied in this work are generally arranged in a monolayer within the interlayer. The poly(propylene oxide) backbones of the molecules are arranged along the midplanes of the interlayer and the orientation of the headgroups depends on whether an ammonium or amine group is present. The arrangement of the PPO backbone contrasts with the behavior of poly(ethylene oxide)-based polymers previously studied, which are hydrophilic and arrange themselves along the face of the clay sheets to form bilayers.[15,16] Despite the difference in conformation between ammonium and amine headgroups, the interlayer spacing in the simulated systems does not vary in a systematic way as might be expected. This is due to the effect that the Na^+ cations have on the structure, as each ammonium headgroup results in one less Na^+ cation. The Na^+ cations and associated water occupy a significant amount of interlayer space, offsetting the less bulky conformation of the amine group.

As discussed, in molecular dynamics simulations the amphiphilic nature of the Na^+-montmorillonite is influenced by the presence of organoammonium species, the orientation of water molecules within the interlayer depending upon whether the monomers were terminated with ammonium or amine groups, due to the changes in hydrogen-bonding networks and absence of Na^+ cations which might otherwise coordinate the water strongly.

Experimentally, it has been shown that the increase in N−H bending mode frequency in the FTIR spectra in the interlayer of amine intercalated clays is *not* a result of formation of ammonium ions followed by hydrogen bonding between the ammonium ion H atoms and siloxane surface O atoms of the clay sheet but arises in composites containing *mixtures* of amine and ammonium species. Computer simulations suggest that these high-frequency FTIR shifts may be due to the strong inter- and intramolecular hydrogen-bonding between ammonium ion H atoms and amine N atoms. Simulated FTIR spectra could be computed from the molecular dynamics simulations using, for example, velocity autocorrelation functions, but these methods are computationally intensive and, as such, not carried out here.[51]

The presence of amine functional groups in the interlayer suggests that, in other studies, further in situ condensation reactions may be possible with, for example, poly(ethylene glycol) monomers. The simultaneous presence of ammonium ions should result in a very strong interaction between clay and intercalated polymer.

The present study shows that the interplay between the monomer headgroup, cation exchange capacity of the clay, and monomer backbone all play a role in determining the interlayer arrangement. However, using our present approach where periodic boundary conditions imply infinite clay sheets, it is not possible to simulate intercalation processes. Rather, it is assumed that our periodic models represent the equilibrium interlayer distribution of water and organic molecules. Mesoscopic simulation studies have suggested that this assumption may be limiting, as in instances where monomers have headgroups which strongly interact with the clay sheets, such as ammonium groups for instance, and long water-soluble backbones, the headgroups do not intercalate very well but remain at the edges of the clay sheets while the long backbone penetrates far into the clay interlayer.[52] This may explain why it is not possible to exchange all the Na^+ ions in Na^+-montmorillonite and appears to be corroborated by a study by Lin and Chen, who determined that mica clay platelets with higher aspect ratios intercalate less material than montmorillonite platelets, which have similar cation exchange capacity but lower aspect ratios.[28] The presence of Na^+ (and other) cations in the interlayer of these systems could also result in "pinning" taking place whereby the low interlayer spacing results in the clay sheets being restrained from separating by their Coulombic attraction to the cations.[53] Xiao et al. have shown that the size of this effect increases with decreasing monomer size for alkylamines.[30]

In summary, we have illustrated the usefulness of large-scale molecular dynamics simulations for gaining an understanding of experimental data for these hard to characterize materials. We have been able to rationalize FTIR data by showing that it is unlikely that alkylamines are intercalated from solution as either pure amine or pure ammonium species, but rather as a mixture of the two. Simulations show that, surprisingly, amine functional groups do not interact strongly with the clay sheets of montmorillonite, whereas ammonium groups do, causing a conformational change in the organic molecule. Further research will explore the novel aluminosilicate sheet undulations encountered in the large-scale molecular dynamics simulations, which should provide a handle for calculating various mechanical and other material properties for such clay−polymer nanocomposites.

Acknowledgment. We thank Prof. J. R. G. Evans and B. Chen at Queen Mary University of London for useful discussions. We are grateful to the Engineering and Physical Sciences Research Council for supporting this work under Grant GR/R30907, which also provided access to the supercomputing facilities at CSAR (Manchester, U.K.), as well as to HEFCE for funding an SGI Onyx 2 at UCL, and Accelrys Inc. for providing software. We also thank Dr. D. G. Apperley at Durham University for help with solid-state NMR and Dr. Dave Konerding (Lawrence Berkeley National Laboratory) for assistance with Chimera.

References and Notes

(1) (a) Pinnavaia, T. J., Beall, G. W., Eds.; *Polymer-Clay Nanocomposites*; John Wiley & Sons Ltd.: Chichester, 2000. (b) Giannelis, E. P. *Adv. Mater.* **1996**, 8, 29−35. (c) Theng, B. K. G. *The Chemistry of Clay-Organic Reactions*; John Wiley and Sons: New York, 1974; Chapters 3 and 4.
(2) Chen, B. *Br. Ceram. Trans.* **2004**, *103*, 241−249.
(3) Bowden, A. A.; Chen, B. Q.; Coveney, P. V.; Evans, J. R. G.; Greenwell, H. C.; Whiting, A. Morphology and mechanical properties of novel poly[oligo(ethylene glycol) diacrylate]-clay nanocomposites. Manuscript in preparation.

(4) Bloys, B.; Davis, N.; Smolen, B.; Bailey, L.; Houwen, O.; Reid, P.; Sherwood, J.; Fraser, L.; Hodder, M. *Schlumberger Oilfield Rev.* **1994**, *6*, 33−43.
(5) Boek, E. S.; Coveney, P. V.; Craster, B.; Reid, P. I. In *Chemicals in the oil industry: recent developments: proceedings of the sixth international symposium on chemistry in the oil industry;* Cookson, L., Ogden, P. H., Eds.; Royal Society of Chemistry: Cambridge, 1999.
(6) Bains, A. S.; Boek, E. S.; Coveney, P. V.; Williams, S. J.; Akbar, M. V. *Mol. Simul.* **2001**, *26*, 101.
(7) Coveney, P. V.; Watkinson, M.; Whiting, A.; Boek, E. S. Stabilizing Clayey Formations. US Patent Number 6,787,-507.
(8) Lan. T.; Kaviratna, P.; Pinnavaia, T. J. *J. Phys. Chem. Solids* **1996**, *57*, 1005−1010.
(9) Kozak, M.; Domka, L. T. *J. Phys. Chem. Solids* **2004**, *65*, 441−445.
(10) Wieczorek, M.; Krysztafkiewicz, A.; Jesionowski, T. *J. Phys. Chem. Solids* **2004**, *65*, 447−452.
(11) Gatos, K. G.; Thorman, R.; Karger-Kocsis, J. *Polym. Int.* **2004**, *53*, 1191−1197.
(12) Yoon, P. J.; Hunter, D. L.; Paul, D. R. *Polymer* **2003**, *44*, 5323−5339.
(13) Yariv, S. In *Organo-Clay Complexes and Interactions*; Yariv, S., Cross, H., Eds.; Marcel Dekker: New York, 2002; Chapter 8.
(14) Greenwell, H. C.; Stackhouse, S.; Coveney, P. V.; Jones, W. Molecular modelling of the structure and properties of clays: A materials chemistry perspective. Manuscript in preparation.
(15) Boulet, P.; Bowden, A. A.; Coveney, P. V.; Whiting, A. *J. Mater. Chem.* **2003**, *13*, 2540−2550.
(16) Boulet, P.; Bowden, A. A.; Chen, B. Q.; Coveney, P. V.; Evans, J. R. G.; Greenwell, H. C.; Whiting, A. Intercalation and in situ polymerization of poly(alkylene oxide) derivatives within M^+-montmorillonite (M= Li, Na, K). Manuscript in preparation.
(17) Zeng, Q. H.; Yu, A. B.; Lu, G. Q.; Standish, R. K. *Chem. Mater.* **2003**, *15*, 4732−4738.
(18) Zeng, Q. H.; Yu, A. B.; Lu, G. Q.; Standish, R. K. *J. Phys. Chem. B* **2003**, *15*, 10025−10033.
(19) Pospíšil, M.; Čapková, P.; Měřínská, D.; Maláč, Z.; Šimoník, J. *J. Colloid Interface Sci.* **2001**, *236*, 127−131.
(20) Heinz, H.; Suter, U. W. *J. Phys. Chem. B* **2004**, *108*, 18341−18352.
(21) Heinz, H.; Castelijns, H. J.; Suter, U. W. *J. Am. Chem. Soc.* **2003**, *125*, 9500−9510.
(22) Pospíšil, M.; Kalendová, A.; Čapková, P.; Šimoník, J.; Valásková, M. *J. Colloid Interface Sci.* **2004**, *277*, 154−161.
(23) Lin, J.-J.; Cheng, I.-J.; Wang, R.; Lee, R.-J. *Macromolecules* **2001**, *34*, 8832−8834.
(24) Lin, J.-J.; Chen, I.-J.; Chou, C.-C. *Macromol. Rapid Commun.* **2003**, *24*, 492−495.
(25) Chou, C.-C.; Shieu, F.-S.; Lin, J.-J. *Macromolecules* **2003**, *36*, 2187−2189.
(26) Lin, J.-J.; Chou, C.-C.; Lin, J.-L. *Macromol. Rapid Commun.* **2004**, *25*, 1109−1112.
(27) Chou, C.-C.; Chang, Y.-C.; Chiang, M.-L..; Lin, J.-J. *Macromolecules* **2004**, *37*, 473−477.
(28) Lin, J.-J.; Chen, Y.-M. *Langmuir* **2004**, *20*, 4261−4264.
(29) Lin, J.-J.; Chang, Y.-C.; Chen, I.-J. *Macromol. Rapid Commun.* **2004**, *25*, 508−512.
(30) Xiao, W.; Zhan, M.; Li, Z. *Mater. Design* **2003**, *24*, 455−462.
(31) Pironon, J.; Pelletier, M.; de Donato, P.; Mosser-Ruck, R. *Clay Miner.* **2003**, *38*, 201−211.
(32) Plimpton, S. Large-scale atomic/molecular massively parallel simulator; http://www.cs.sandia.gov/~sjplimp/lammps.html., Sandia National Laboratories, Albuquerque, 2001.
(33) Plimpton, S. *J. Comput. Phys.* **1995**, *117*, 1−19.
(34) Boulet, P.; Coveney, P. V.; Stackhouse, S. *Chem. Phys. Lett.* **2004**, *389*, 261−267.
(35) Hein, J.; Reid, F.; Smith, L.; Bush, I.; Guest, M.; Sherwood, P. On the performance of molecular dynamics applications on current high-end systems. in press.
(36) Hockney, R. W.; Eastwood, J. *Computer Simulation Using Particles*; MacGraw-Hill: New York, 1981.
(37) Luty, B. A.; Davis, M. E.; Tironi, I. G.; Vangunsteren, W. F. *Mol. Simul.* **1994**, *14*, 11−20.
(38) Rajagopal, G.; Needs, R. J. *J. Comput. Phys.* **1994**, *115*, 399−405.
(39) Toukmaji, A. Y.; Board, J. A. *Comput. Phys. Commun.* **1996**, *95*, 73−92.
(40) Tuckerman, M.; Berne, B. J.; Martyna, G. J. *J. Chem. Phys.* **1992**, *97*, 1990−2001.
(41) Teppen, B. J. Private communication, 2002.
(42) Teppen, B. J.; Rasmussen, K.; Bertsch, P. M.; Miller, D. M.; Schafer, L. *J. Phys. Chem. B* **1997**, *101*, 1579−1587.
(43) Greenwell, H. C.; Coveney, P. V.; Harvey, M. J. *Geochim. Cosmochim. Acta* **2004**, *68*, A106.
(44) UCSF Chimera package, Computer Graphics Laboratory, University of California, San Francisco (supported by NIH P41 RR-01081). Pettersen, E. F.; Goddard, T. D.; Huang, C. C.; Couch, G. S.; Greenblatt, D. M.; Meng, E. C.; Ferrin, T. E. *J. Comput. Chem.* **2004**, *25*, 1605−1612.
(45) Li, J. *Modelling Simul. Mater. Sci. Eng.* **2003**, *11*, 173−177.
(46) Yariv, S. Heller, L. *Isr. J. Chem.* **1970**, *8*, 391.
(47) Yariv, S.; Shoval S. *Clays Clay Miner.* **1979**, *27*, 29−38.
(48) Lindahl, E.; Edholm, O. *Biophys. J.* **2000**, *79*, 426−433.
(49) Stackhouse, S.; Coveney, P. V.; Sandré, E. *J. Am. Chem. Soc.* **2001**, *123*, 11764−11774.
(50) Greenwell, H. C.; Stackhouse, S.; Coveney, P. V.; Jones, W. *J. Phys. Chem. B* **2003**, *107*, 3476−3485.
(51) Stackhouse, S.; Coveney, P. V.; Benoit, D. M. *J. Phys. Chem. B* **2004**, *108*, 9685−9694.
(52) Sinsawat, A.; Anderson, K. L.; Vaia, R. A.; Farmer, B. L. *J. Polym. Sci., Part B* **2003**, *41*, 3272−3284.
(53) Shi, H.; Lan, T.; Pinnavaia, T. J. *Chem. Mater.* **1996**, *8*, 1584−1589.

MA0503817